Supplementary Information
"Dynamics of $[Pyr_{13}][Tf_2N]$ ionic liquid confined to carbon black"

Steffen Merz,* Peter Jakes, Svitlana Taranenko, Rüdiger-A. Eichel, Josef Granwehr

SI–1. Parametrization of Laplace inversion

The Laplace inversion for the different data sets was parametrized as described in [I]. First, the data was scaled to unity variance using the standard deviation of data points with no signal, *i.e.* points that solely contained noise. Although this procedure only provides an estimate of the noise level – while random noise is usually frequency independent within the bandwidth detected in a high-field NMR experiment, multiplicative or t_1 noise[2] cannot be ruled out *a priori* – it is generally sufficient, since parametrization of the uniform penalty (UP) algorithm is not oversensitive to the exact parameter choice[3].
Inversion of data was done using an exponential kernel and a generalized Tikhonov regularization with UP and an additional zero-crossing (ZC) penalty. No singular-value-decomposition-based data compression as described by Venkataramanan *et al.*[4] was performed. The parameters of the uniform penalty inversion were chosen algorithmically as suggested in [I] and summarized in Table S1:

Table S1: List of parameters used for Laplace inversion of T_1 and diffusion data.

Parameter name	Parameter symbol[1]	Value
Global scaling factor	λ	1
Curvature compliance	α_c	$R\Delta_r \prod_{\rho=1}^{R} \frac{M_\rho}{N_\rho}$
Slope compliance	α_p	$5\alpha_c$
Floor compliance	α_0	10^{-4}
Averaging parameter (for UP and ZC)	η	1
Zero crossing weight	α_d	10^{-5}
Zero crossing limit	α_D	0
Boundary regularization width	h_0	2
Boundary regularization weight	α_a	$50/\Delta_r$
Boundary regularization limit	α_A	0

R number of dimensions of data set
Δ_r spacing between data points along dimension r
M_ρ number of points of discretized distribution function along dimension ρ
N_ρ number of data points along dimension ρ

The ZC coefficients were limited by the respective coefficient of the UP matrix, hence α_D was set to zero. For the non-inverted spectral dimension, the axis was defined by simply numbering the data points consecutively, thus $\Delta_r = 1$. Furthermore, no boundary penalty was applied along non-inverted dimensions, *i.e.* $h_0 = 0$.

*e-mail: s.merz@fz-juelich.de

SI–2. Testing suitability of non-negativity constraint for T_1 data

A straightforward method to test the suitability of different parametrizations for Laplace inversion is to compare their residuals. For the ^{1}H NMR inversion–recovery (IR) data of the [Pyr_{13}] cation data of [Pyr_{13}][Tf_2N] ionic liquid (IL) in Vulcan XC-72 carbon black is shown in Fig. S1.

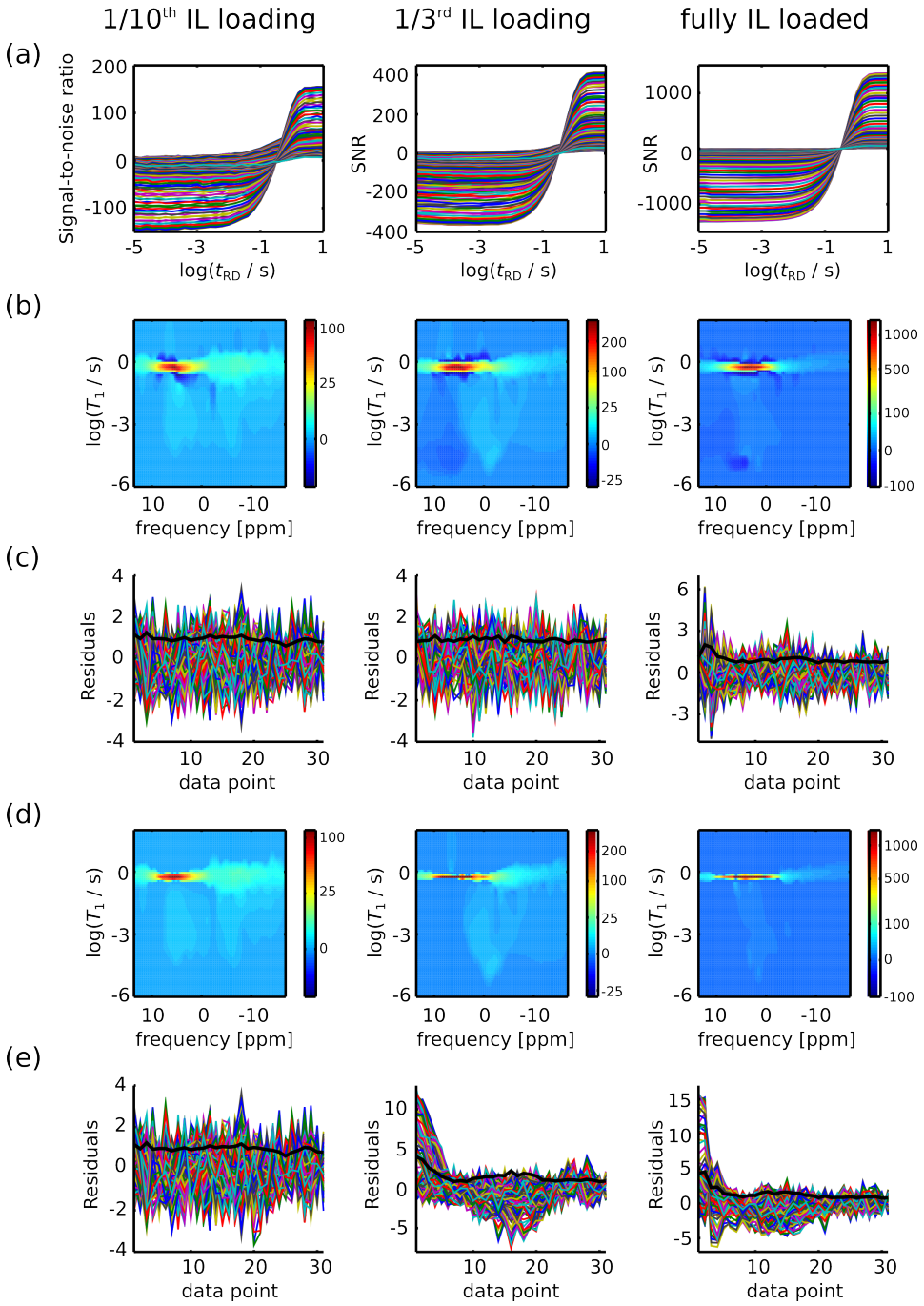

Figure S1: Analysis of IR data from samples with different pore space loading of VXC-72 carbon black with [Pyr_{13}][Tf_2N] IL. (a) Raw data, normalized to unity noise variance. (b) T_1 relaxation time distribution *vs.* ^{1}H NMR frequency as presented in the main text, obtained using UP regularization and an additional ZC penalty, but without non-negativity constraint. (c) Residuals of the fit plotted along the recovery time dimension (coloured lines) and standard deviation of the different spectral data points for each recovery time (black). (d) T_1 relaxation time distribution *vs.* ^{1}H NMR frequency, obtained using an additional non-negativity penalty[3]. (e) Residuals of the fit plotted along the recovery time dimension for the fit with non-negativity penalty.

In Fig. S1a, the signal is normalized to unity variance, hence it directly represents the signal-to-noise ratio (SNR). As expected for data sets recorded with identical parameters, the SNR is approximately proportional to the pore space loading. All inverted spectra show negative features, although with relatively low amplitude (the colour map values are scaled with the square root of their respective amplitude, but retaining their sign). For all data sets, the obtained distributions show negative features in the immediate vicinity of the main relaxation mode. Although these features can be reproduced when the experiments are repeated, moderate undershooting is not uncommon for data with relatively high SNR and needs to be analyzed carefully to avoid overinterpretation[3]. On the other hand, the weak negative features appearing at short T_1 values for the samples with intermediate and with full pore space loading are characteristic and indicate a physical origin.

The accuracy of the inversion can be visualized by plotting the residuals of the fit (Fig. S1c). Ideally, only independent and identically distributed (iid) Gaussian white noise without any apparent features should be obtained. This can be observed for the samples with 1/10th and 1/3rd of the pore space loaded. At full pore space loading, however, there are moderate deviations from random noise, which indicate that the conducted inversion was not able to reproduce all features contained in the data. This can be observed if the kernel is not capable of reproducing all the signal components. In NMR, this can be the case if data contains exponential as well as Gaussian features. Inversion with the standard parametrization then leads to oscillating features in the distribution, and non-random patterns or significant deviations from white noise are found in the residuals. A more aggressive regularization can suppress these residuals, but the obtained distribution becomes unstable. In the present case, only the fully loaded sample shows significant deviations from iid white noise. These deviations are primarily located at recovery times $t_{\mathrm{RD}} < 10^{-4}$ s and, to a lesser extent, at $t_{\mathrm{RD}} \approx 10^{-2}$ s. Changes on this timescale are most probably originating from IL cations that are exchanging between different environments. Given the non-uniform surface structure and morphology of carbon black, non-exponential contributions in the T_1 distribution are plausible.

When processing the identical data with an additional non-negativity penalty, the negative features disappear for all three data sets and the relaxation modes narrow (Fig. S1d). Considering the residuals (Fig. S1e), the sample with 1/10th pore space loading, which shows weak exchange features (see main text), displays only weak changes in the residuals. Hence at the available SNR, negative features do not appear to be necessary to reproduce the data. However, at 1/3rd pore space loading, the residuals show pronounced non-random patterns. In this case, negative features, although weak in amplitude, are necessary for a consistent reproduction of the data. Hence the features appearing at $T_1 \sim 10^{-4}$ s are significant. At full pore space loading, the residuals are again less affected by non-random features. This is consistent with Fig. 1b in the main text where the sample with a pore space loading of 1/3rd shows strong exchange features and can on average be considered to be at the transition between slow and fast exchange. Overall, these data indicate that for these experiments a non-negativity constraint should be avoided. Considering that the feature width in the T_1 distribution changes if a constraint is imposed, the same processing parameters need to be employed for all data sets to achieve a reliable comparability of the data, even though for the 1/10th IL loaded sample a non-negativity constraint does not significantly alter the residuals.

SI–3. Testing suitability of non-negativity constraint for diffusion data

A comparison of the Laplace inversion without and with non-negativity penalty for the diffusion data of the sample with 1/3rd pore space loading is shown in Fig. S2.

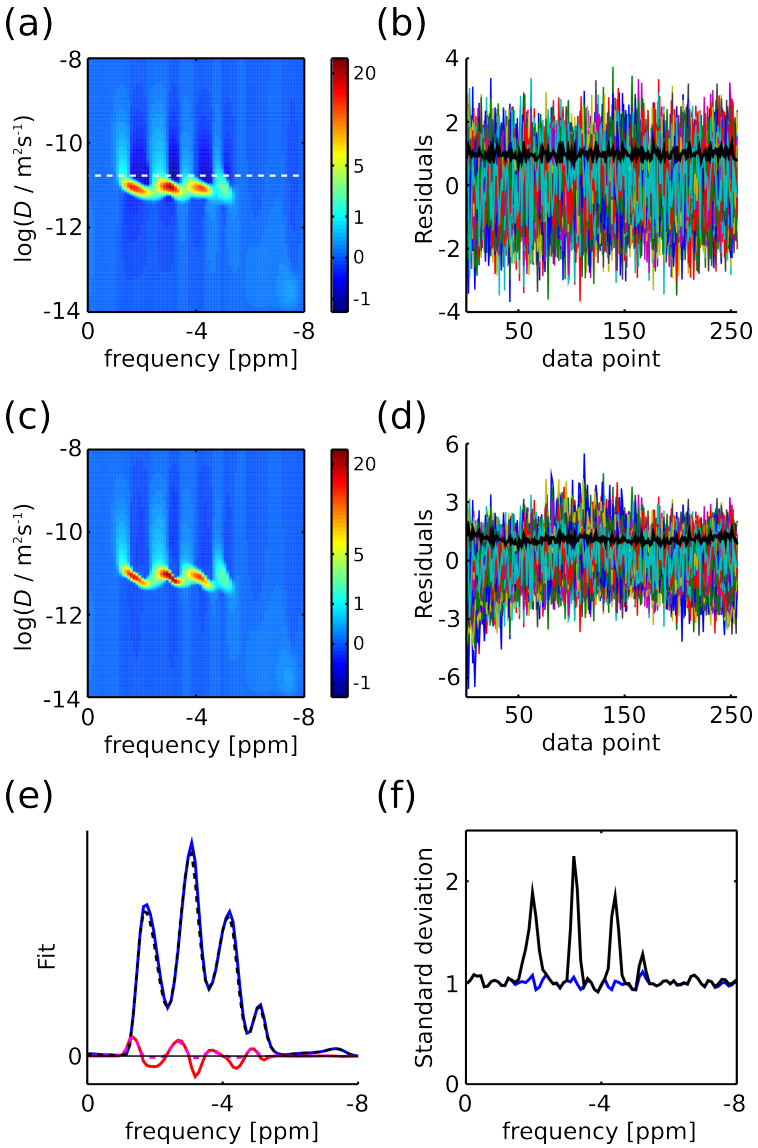

Figure S2: Analysis of ^{1}H NMR diffusion data from a VXC-72 carbon black sample with 1/3rd of the pore space loaded with [Pyr_{13}][Tf_2N] IL. (a) Diffusion coefficient distribution *vs.* ^{1}H NMR frequency as presented in the main text, obtained using a UP regularization and an additional ZC penalty without non-negativity constraint. The dashed white line represents the boundary chosen to calculate a fast and regular contribution to the fit. (b) Residuals of the fit plotted along the gradient strength dimension (coloured lines) and standard deviation from the different spectral data points for each gradient value (black). The data was normalized to unity noise. (c) Diffusion coefficient distribution *vs.* ^{1}H NMR frequency, obtained applying an additional non-negativity penalty[3]. (d) Residuals of the fit plotted along the gradient strength dimension for the fit with non-negativity penalty. (e) Contributions to the fit from signal components in the diffusion distribution below $D = 1.58^{-11}$ m^2/s (blue solid line for inversion without non-negativity penalty and black dashed line for inversion with non-negativity penalty) and above $D = 1.58^{-11}$ m^2/s (red solid line for inversion without non-negativity penalty and magenta dashed line for inversion with non-negativity penalty). (f) Standard deviation from the different points in the gradient strength dimension plotted along the spectral dimension (blue for inversion without non-negativity penalty and black for inversion with non-negativity penalty).

The distributions of diffusion coefficients with and without non-negativity penalty (Fig. S2a,c) show the same main features except for the negative components at fast D. Comparing the residuals (Fig. S2b,d), the negative components in the distribution are clearly supported by the data and therefore considered significant despite their low amplitude. On the other hand, since the positive and negative features are well separated the same positive features appear in both distributions, *i.e.* no artificial features occur in the distribution obtained with a non-negativity penalty. This is also highlighted when comparing the standard deviation of the residuals calculated along the gradient strength dimension and plotted *vs.* the ^{1}H NMR frequency (Fig. S2f). At frequencies with negative components in the distribution the standard deviation of the non-negativity penalized spectrum increase significantly, while at other frequencies both data sets show identical deviations.
The contribution to the overall signal from the component with fast D can be obtained by forward calculating part of the distribution. In Fig. S2e the contributions above and below the white dotted line in Fig. S2a are compared. Albeit not dominant, the fast moving components clearly contribute to the signal by a significant fraction. Again, when comparing the contribution without and with non-negativity penalty, the positive part of the signal is essentially constant.

SI–4. Effect of exchange on spectra and relaxation distribution

To demonstrate the effects of exchange on T_1 relaxation *vs.* NMR frequency 2D spectra, numerical simulations of a two-spin system with slow and with fast exchange were conducted (Fig. S3). The simulations were performed using classical equations of motion with an exchange term.[5] These simulations are used to illustrate arguments used in the main text but are not representative for the investigated IL system that shows a more complex exchange behaviour between multiple sites.

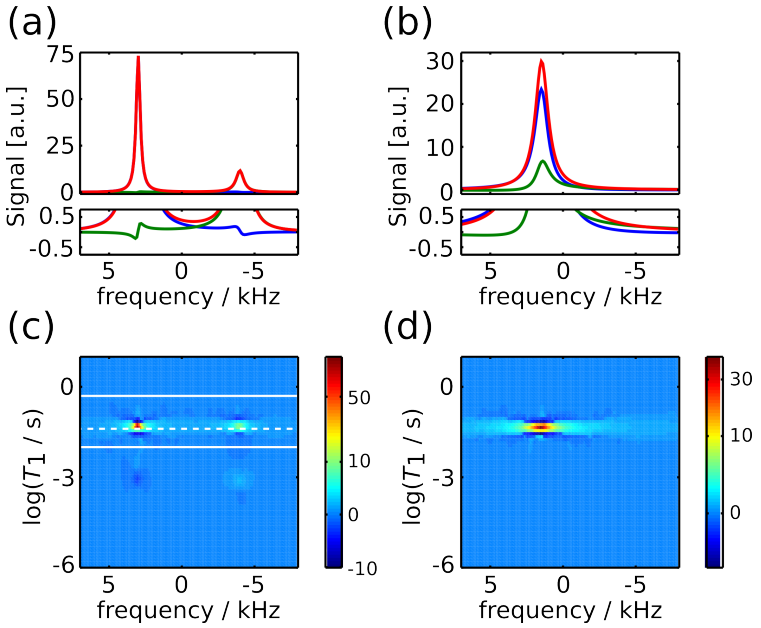

Figure S3: Numerical simulation of two-site exchange for slow (a,c) and fast (b,d) exchange. (a,b) NMR spectrum (red), with the individual spectra of spin A (blue) and spin B (green). The upper panels show the full spectrum, the lower panels zoom in onto the base of the spectra. (c,d) T_1 distribution *vs.* NMR frequency. The solid white lines in (c) mark the position of T_1 of the two spins, the dashed line represents the inverse weighted mean of the relaxation rates.

The parameters used for the simulation are summarized in Table S2:

Table S2: Parameters used to simulate an IR experiment for a two-site spin system with exchange.

Parameter name	Parameter symbol	Value
Resonance frequency spin A	ν_A	3.0 kHz
Resonance frequency spin B	ν_B	−4.0 kHz
Spin–lattice relaxation time spin A	$T_{1,A}$	0.5 s
Spin–lattice relaxation time spin B	$T_{1,B}$	0.01 s
Spin–spin relaxation time spin A	$T_{2,A}$	1.3 ms
Spin–spin relaxation time spin B	$T_{2,B}$	1.0 ms
Magnetization ratio	$\frac{M_{0,A}}{M_{0,B}}$	1 : 0.3
Exchange rate A → B slow	$k_{AB}^{(\mathrm{slow})}$	300 s^{-1}
Exchange rate B → A slow	$k_{BA}^{(\mathrm{slow})}$	$k_{AB}^{(\mathrm{slow})}\frac{M_{0,A}}{M_{0,B}} = 1000\ \mathrm{s}^{-1}$
Exchange rate A → B fast	$k_{AB}^{(\mathrm{fast})}$	$100 \times k_{AB}^{(\mathrm{slow})} = 30000\ \mathrm{s}^{-1}$
Exchange rate B → A fast	$k_{BA}^{(\mathrm{fast})}$	$100 \times k_{BA}^{(\mathrm{slow})} = 100000\ \mathrm{s}^{-1}$
Recovery delays	t_{RD}	101 pts., log spaced between 10^{-6} s and 100 s

As expected, for slow exchange the two resonances are well separated while for fast exchange coalescence at the position of the weighted mean frequency is observed (Fig. S3a,b). One cause for negative components in the relaxation distribution can be seen even in this simple example: the individual spectrum of each of the

two spins shows a weak resonances at the position of the respective other spin but phase shifted. At least part of such a contribution will necessarily relax with opposite sign compared to the main resonance.
If complete coalescence occurs (Fig. S3d), a spectrum similar to a single-component spectrum is observed. For slow exchange without coalescence and exchange faster than relaxation, an additional mode appears in the relaxation distribution that approximately enables an estimate of exchange rates (Fig. S3c).

Notes and references

[1] J. Granwehr, P.J. Roberts, *J. Chem. Theory Comput.* **8**, 3473–3482 (2012).

[2] J. Granwehr, *Appl. Magn. Reson.* **32**, 113–156 (2007).

[3] G.C. Borgia, R.J.S. Brown, P. Fantazzini, *J. Magn. Reson.* **132**, 65–77 (1998).

[4] L. Venkataramanan, Y.-Q. Song, M.D. Hürlimann, *IEEE Trans. Signal Process.* **50**, 1017–1026 (2002).

[5] M. van Landeghem, A. Haber, J.-B. d'Espinose de Lacaillerie, B. Blümich, *Concepts Magn. Reson. A* **36**, 153–169 (2010).